An efficient model development and experimental study for the heat transfer in naturally ventilated inclined roofs

Shanshan Tong, Hua Li*

School of Mechanical and Aerospace Engineering, Nanyang Technological University,

50 Nanyang Avenue, Singapore 639798, Republic of Singapore

Abstract

Roof ventilation is an efficient way to reduce the heat transmission into building interior in summer. In this work, a theoretical model is developed to predict the heat flux transferred through the naturally ventilated inclined roof in a fast and accurate manner. In particular, the thermal resistance due to the coupled radiation and convection in roof cavity is modeled using the circuit transformation theory. Moreover, based on the computational fluid dynamics (CFD) analysis, correlations are proposed for the convective resistances in the naturally ventilated inclined cavity. Laboratory experiments are further carried out to validate the CFD model, and a satisfactory agreement is found between the experimentally measured and numerically simulated airflow velocity and temperature in the cavity. In order to evaluate the accuracy of developed model, the heat flux transferred into building interior is predicted by both the developed model and a full CFD model. A good agreement is achieved between the predictions of the two models. Based on the developed model, parametric studies are conducted to investigate the influences of key roof parameters on the heat flux transferred into building interior. Ranked in order of significance, the influential parameters are the solar reflectance of exterior roof surface, infrared emittance of cavity surface, thermal resistance of lower roof slab, thermal resistance of upper roof slab, roof inclination and cavity spacing.

Keywords: Roof heat gain, Natural ventilation, Thermal resistance circuit, Heat transfer modeling.

Corresponding author: Hua Li, Tel.: (+65)6790 4953, Email address: lihua@ntu.edu.sg

Postal address: School of Mechanical and Aerospace Engineering, Nanyang Technological University, 50 Nanyang Avenue, Singapore 639798, Republic of Singapore

1. Introduction

In recent years, the naturally ventilated roofs were widely studied due to their remarkable merits in reducing the solar heat gain and improving the indoor thermal comfort in summer. A common ventilated roof consists of two parallel solid slabs and a delimited open-ended air cavity between the two slabs. An upward flow is formed inside the roof cavity due to buoyancy force, which contributes to carry out part of the accumulated heat accumulated in the roof and cut down the heat transmission into building interior.

A literature review reveals that many experimental and theoretical studies have been carried out to evaluate the thermal behaviour of naturally ventilated roofs. Most experimental studies on the ventilated roofs involved the measurements of roof surface temperature, airflow temperature and velocity, or heat flux transferred across the upper and lower roof slabs. For example, Dimoudi et al. [1] performed a field experiment on a full-scale roof in the summer of Greece in 2006. They examined the effects of roof ventilation and radiant barrier on the roof heat gain. It was found that the application of a 6-cm ventilated cavity reduced the roof heat gain by 56% during the daytime compared with an unventilated roof. The radiant barrier with the low infrared emittance effectively reduced the radiative heat transfer from upper to lower cavity surface, and thus increased the daily heat gain reduction of ventilated roof to 68%. In 2007, Puangsombut et al. [2] carried out experiments on a ventilated roof with uniform heat flux on the upper cavity surface. They examined the airflow rate and convective heat transfer in the inclined roof cavity using two dimensionless parameters: Nusselt and Reynolds numbers. Based on measured data, these two parameters were correlated to three variables: Rayleigh number, roof inclination and aspect ratio. After the application of radiant barrier, it was found that the heat flux transferred through the lower slab reduced by about 50%, and the convective heat transfer and airflow rate in the roof cavity increased by about 40–50%. Lai et al. [3] carried out experiments on a scaled ventilated inclined roof with the upper roof slab heated by a lighting

system. They measured the airflow velocity and temperature in the cavity for different roof inclinations and spacings. A correlation was proposed for the Nusselt number in the ventilated cavity, and an optimum cavity spacing of 10 cm was suggested for the 1-m long roof for the maximum convective heat transfer. In 2008, Chang et al. [4] carried out experiments on an asymmetrically heated ventilated roof for different inclinations and cavity spacings. Based on measured data, they calculated the U-values of ventilated roofs and correlated U-values to the Rayleigh number, roof inclination and cavity aspect ratio. In 2009, Susanti et al. [5] carried out experiments on a 4.8-m long naturally ventilated inclined roof under different heating intensities, and measured the induced airflow velocity and temperature in the cavity with different opening ratios. Moreover, the induced airflow velocity and temperature rise were correlated to the incident heat flux, cavity spacing, roof inclination and opening ratio. In 2011, Roels and Deurinck [6] evaluated the effect of radiant barrier on the thermal performance of ventilated roofs using three methods: laboratory experiments, field testing and numerical modeling. The laboratory experiment and simulation showed that the radiant barrier reduced the daily heat gain of roof effectively, while the field testing revealed that the air-tightness, wind and stack effects were important and could disturb the potential benefits of using a radiant barrier.

Theoretical studies were conducted as well to analyze the thermal performance of naturally ventilated inclined roofs. The computational fluid dynamic (CFD) technique was often used to predict the induced airflow temperature and velocity in ventilated roofs. For example, Biwole et al. [7] numerically modelled the radiative, convective and conductive heat transfers through a ventilated roof, and validated the numerical model using field experiments on a ventilated roof that was formed by adding a metallic screen on a metal roof. They simulated the impacts of various parameters on the energy efficiency of ventilated roofs, including the infrared emittance of sheet metal, solar reflectance of screen, insulation thickness and roof inclination. In 2010, Chami and Zoughaib [8] developed a CFD model to simulate the convective heat transfer in the

roof cavity, and validated the model through measurements on a scaled roof using the particle image velocimetry system. Moreover, correlations were proposed for the induced airflow rate and convective heat transfer coefficient in the cavity. More recently, Gagliano et al. [9] analyzed the impacts of roof ventilation and thermal resistances of roof slabs on the heat flux transferred into building interior using the CFD code Fluent. It was revealed that roof ventilation can reduce almost 50% of transferred heat flux in summer, and the optimum position for the thermal insulation layer is under the air layer adhering to the lower slab. Miller et al. [10] proposed a correlation for the laminar airflow rate in the inclined cavity through CFD analysis, and developed an algorithm to predict the convective heat transfer coefficient in the cavity heated from above or below. In addition to ventilated roofs, CFD technique was used to analyze the laminar [11], transitional [12, 13] and turbulent [14, 15] flow in the naturally ventilated inclined channels or photovoltaic panels as well. In general, CFD techniques provide accurate predictions for the rates of induced airflow and convective heat transfer in the naturally ventilated cavities, whereas they often require heavy computing resources. In order to provide a fast estimation, Ciampi et al. [16] developed an analytical model to analyze the energy savings of ventilated facades using the thermal circuit analysis and Gnielinski correlation [17]. This model was later applied to the energy analysis of ventilated roofs [18]. However, the Gnielinski correlation was developed for the turbulent forced convection in tubes or pipes with circular sections, and it expresses the Nusselt number as a function of the Reynolds number and Darcy friction factor [17]. While the roof cavities are mostly rectangular and the Reynolds number is often unknown for the natural convection flow, it might be inappropriate to use the Gnielinski correlation to estimate the natural convective heat transfer in the roof cavity.

Nevertheless, the fast and accurate determination of the heat flux transferred through the naturally ventilated inclined roof is a great challenge. As shown in Fig. 1, the heat transfers through a ventilated roof are quite complex, including the coupled convective and radiative heat

transfers at the exterior and interior roof surfaces (q_{o} and q_{i}), the conductive heat transfers within the upper and lower roof slabs ($q_{\mathrm{cond,u}}$ and $q_{\mathrm{cond,l}}$), the convective heat transfers at the upper and lower surfaces of cavity ($q_{\mathrm{conv,h}}$ and $q_{\mathrm{conv,c}}$), and the radiative heat transfer from upper to lower surface of cavity (q_{rad}). Among these heat transfers, q_{o} and q_{i} are affected by the thermal resistances of exterior and interior air films, $q_{\mathrm{cond,u}}$ and $q_{\mathrm{cond,l}}$ are affected by the thermal resistances of roof slabs, and q_{rad} is readily predictable using the radiation theory [19]. However, $q_{\mathrm{conv,h}}$ and $q_{\mathrm{conv,c}}$ are difficult to evaluate and affected by various factors, such as cavity aspect ratio, roof inclination, outdoor air temperature, and surface temperatures of cavity walls. The surface temperatures of cavity walls are further affected by the other conductive, radiative and convective heat transfers. Therefore, all these heat transfers should be considered simultaneously to provide an accurate prediction for the heat flux transferred into building interior q_{i}.

In present work, a novel model is developed to predict the heat transfers through a naturally ventilated roof using the circuit transform theory and correlations proposed from CFD simulation. Compared with the existing models, the developed model combines the advantages of analytical approach and numerical simulation, and it is capable of predicting the heat flux transferred into building interior q_{i} with high effectiveness and accuracy. In addition, the convective heat fluxes $q_{\mathrm{conv,h}}$ and $q_{\mathrm{conv,c}}$ are estimated using the correlations which are firstly proposed from the CFD analysis on the turbulent flow in naturally ventilated inclined cavities

2. Model development

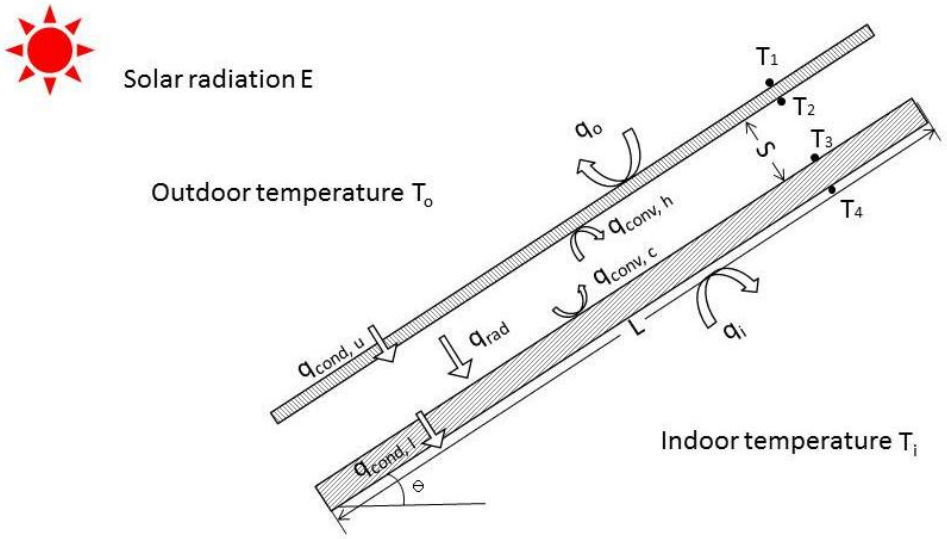

Fig. 1 Heat transfers across a ventilated roof.

Considering a naturally ventilated roof as illustrated in Fig. 1, it is exposed to the solar irradiance E ($\mathrm{W/m^2}$), outdoor air temperature T_o and indoor air temperature T_i. From top to bottom, the surface temperatures of the upper and lower roof slabs are denoted as T_1, T_2, T_3 and T_4 respectively. The thermal network for a ventilated roof is shown in Fig. 2 (a), in which r_e and r_i are the thermal resistances of exterior and interior air films, r_a and r_b are the thermal resistances of upper and lower roof slabs, r_{rad} is the radiative resistance between the upper and lower cavity surface, r_H and r_C are the thermal resistances due to convection between air and the upper or lower roof slabs, and T_a is the sol-air temperature defined as

$$T_a = T_o + \alpha E r_e \tag{1}$$

where α is the dimensionless solar absorptance of exterior roof surface.

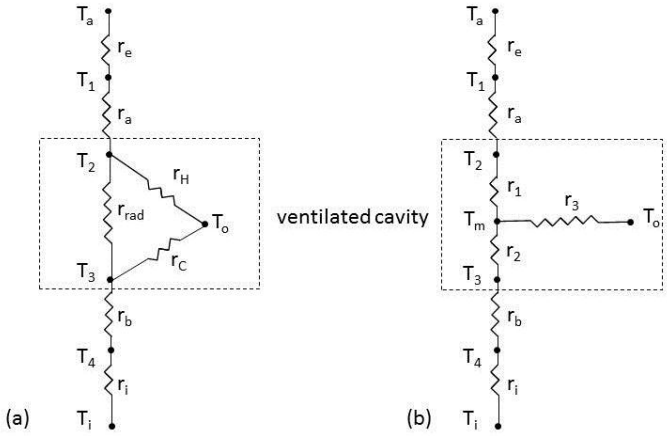

Fig. 2 Thermal networks for the ventilated roof using (a) the triangular circuit and (b) the Y-circuit.

Using the circuit transformation theory [20], the triangular circuit among the temperature nodes T_2, T_3 and T_o in Fig. 2 (a) can be equivalently transformed into the Y-circuit in Fig. 2 (b). According to the transform procedures detailed in Appendix A, the transformed resistances r_1, r_2 and r_3 in Fig. 2 (b) are derived as

$$r_1 = r_H r_{rad} /(r_H + r_{rad} + r_C), \qquad r_2 = r_C r_{rad} /(r_H + r_{rad} + r_C), \qquad r_3 = r_H r_C /(r_H + r_{rad} + r_C) \tag{2}$$

As shown in Fig. 2 (b), a new temperature node T_m is introduced in the Y-circuit, and the heat balance equations at T_2, T_m and T_3 are obtained as

$$T_2: \quad (T_a - T_2)/(r_e + r_a) = (T_2 - T_m)/r_1 \tag{3}$$

$$T_m: \quad (T_2 - T_m)/r_1 = (T_m - T_o)/r_3 + (T_m - T_3)/r_2 \tag{4}$$

$$T_3: \quad (T_m - T_3)/r_2 = (T_3 - T_i)/(r_b + r_i) \tag{5}$$

Solving the Eqs. (3)-(5) for T_2, T_3 and T_m yields

$$T_2 = \frac{r_1 T_a + (r_e + r_a) T_m}{r_e + r_a + r_1} \tag{6}$$

,
$$T_3 = \frac{(r_b + r_i)T_m + r_2 T_i}{r_i + r_b + r_2} \tag{7}$$

$$T_m = \frac{T_a/(r_e + r_a + r_1) + T_o/r_3 + T_i/(r_i + r_b + r_2)}{1/(r_e + r_a + r_1) + 1/r_3 + 1/(r_i + r_b + r_2)} \tag{8}$$

It is observed from Eq. (8) that T_m is the weighted average of temperatures T_a, T_o and T_i with their weights being $1/(r_e + r_a + r_1)$, $1/r_3$ and $1/(r_2 + r_b + r_i)$ respectively.

The heat flux transferred into the building interior (q_i) is thus calculated by

$$q_i = (T_m - T_i)/(r_i + r_b + r_2) \tag{7}$$

In order to estimate the heat flux q_i, it is necessary to determine all the thermal resistances r_e, r_a, r_{rad}, r_H, r_C, r_b and r_i. In general, r_a and r_b are determined by the thermal properties of of roofing materials, and the common values or ranges of r_e.and r_i are suggested by the building thermal codes [21, 22]. For the radiative resistance in the cavity (r_{rad}), it is reasonable to assume that the view factor between the upper and lower slabs is close to 1, since the length and width of cavity are usually much larger than its thickness. Therefore, the radiative resistance r_{rad} becomes [19]

$$r_{rad} = 4\sigma T_w^{\ 3}/(1/e_H + 1/e_C - 1) \tag{8}$$

where σ is the Stefan-Boltzmann constant equal to 5.67×10^{-8} W/(m^2 K^4), T_w is the average of cavity surface temperatures and $T_w = (T_2 + T_3)/2$, and e_H and e_C are the infrared emittance of the upper and lower cavity surfaces respectively.

However, little work is found available in literature regarding the convective resistances r_{H} and r_{C}, though many studies have been done to predict the overall convective heat transfer in the naturally ventilated inclined cavities [11, 14]. The CFD analysis is thus employed to evaluate r_{H} and r_{C} in the following section.

3. CFD simulation

In this section, the CFD technique is employed to analyze the airflow movement and convective heat transfer in the inclined roof cavity. This analysis is mainly restrained to the natural convection flow in the inclined cavities heated from above, so as to mimic the thermal performance of ventilated roofs in summer.

3.1 CFD model

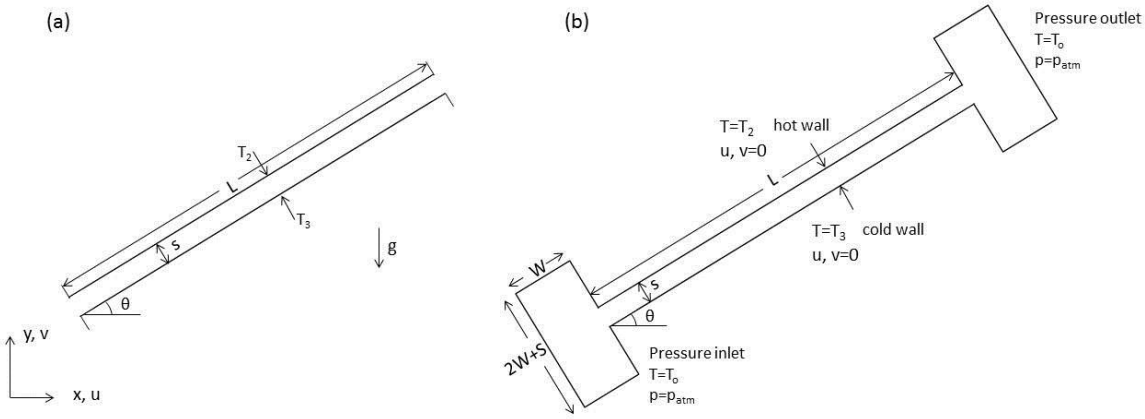

Fig. 3 (a) Geometry and coordinate system of the problem, (b) computational domain and boundary conditions.

The geometry and coordinate system of the analyzed problem are shown in Fig. 3 (a). The ventilated roof is formed by two large parallel slabs of length L, spacing S and inclination angle θ. According to literature [8], the Grashof number based on the cavity length L is generally used to determine the flow regime, and it is calculated by

$$Gr_L = g\beta(T_{\mathrm{w}} - T_{\mathrm{o}})L^3 / \nu^2 \tag{11}$$

in which g is the gravity acceleration in $\mathrm{m/s^2}$, β is the thermal expansion coefficient of air in 1/K, and ν is the kinematic viscosity of air in $\mathrm{m^2/s}$. The natural convection flow typically transits from laminar to turbulent regime when Gr_L falls in the range of $10^9 - 10^{10}$ [13, 23]. If we consider a roof with its length (L) in the range of 1.5-10 m and temperature difference $(T_\mathrm{w} - T_\mathrm{o})$ in the range of 15-30 K, the resulting Gr_L estimated by Eq. (11) falls in the range of $10^9 - 10^{12}$. Therefore, the airflow in the cavity generally reaches the stage of transitional or early turbulent.

Regarding the computational domain, the air pressure and temperature at the cavity inlet or outlet are unknown and different from those of air at rest due to buoyancy force and convective heat transfer [24]. Therefore, an I-type computational domain is adopted to accommodate the momentum and energy diffusion that could occur at the cavity inlet or outlet [9, 25, 26], as shown shown in Fig. 3 (b). Regarding the boundary conditions, the atmospheric pressure ($P = P_\mathrm{atm}$) and outdoor air temperature ($T = T_\mathrm{o}$) are applied at the boundaries of cavity inlet and outlet. The turbulent kinetic energy k and energy dissipation rate ε are set close to zero at the inlet. The turbulent quantities at the cavity outlet are extrapolated from the interior. No-slip conditions are imposed on the upper and lower walls.

The two-equation standard $k-\varepsilon$ model is selected to model the turbulence in the cavity as suggested in the previous studies [8, 9, 13], due to its good convergence rate and relatively low memory requirements compared with the $k-\varepsilon$ and Spalart-Allmaras models [27]. The two-dimensional governing equations for the turbulent flow are listed below.

Conservation of mass (continuity)

$$\frac{\partial(\rho u)}{\partial x} + \frac{\partial(\rho v)}{\partial y} = 0 \tag{12}$$

Conservation of momentum in the x direction

$$\frac{\partial(\rho uu)}{\partial x}+\frac{\partial(\rho uv)}{\partial y}=-\frac{\partial P}{\partial x}+\frac{\partial}{\partial x}\left[(\mu+\mu_{\mathrm{t}})\frac{\partial u}{\partial x}\right]+\frac{\partial}{\partial y}\left[(\mu+\mu_{\mathrm{t}})\frac{\partial u}{\partial y}\right]-\frac{2}{3}\rho\frac{\partial k}{\partial x} \tag{13}$$

Conservation of momentum in the y direction

$$\frac{\partial(\rho uv)}{\partial x}+\frac{\partial(\rho vv)}{\partial y}=-\frac{\partial P}{\partial y}+\frac{\partial}{\partial x}\left[(\mu+\mu_{\mathrm{t}})\frac{\partial v}{\partial x}\right]+\frac{\partial}{\partial y}\left[(\mu+\mu_{\mathrm{t}})\frac{\partial v}{\partial y}\right]-\frac{2}{3}\rho\frac{\partial k}{\partial y}+(\rho-\rho_0)g \tag{14}$$

Conservation of energy

$$\frac{\partial(\rho uT)}{\partial x}+\frac{\partial(\rho vT)}{\partial y}=\frac{\partial}{\partial x}\left[(\frac{\mu}{\mathrm{Pr}}+\frac{\mu_t}{\sigma_t})\frac{\partial T}{\partial x}\right]+\frac{\partial}{\partial y}\left[(\frac{\mu}{\mathrm{Pr}}+\frac{\mu_t}{\sigma_t})\frac{\partial T}{\partial y}\right] \tag{15}$$

The distribution of turbulent kinetic energy k and the dissipation rate of turbulent kinetic energy ε are determined by the transport equations below.

$$\frac{\partial(\rho uk)}{\partial x}+\frac{\partial(\rho vk)}{\partial y}=\frac{\partial}{\partial x}\left[\left(\mu+\frac{\mu_{\mathrm{t}}}{\sigma_k}\right)\frac{\partial k}{\partial x}\right]+\frac{\partial}{\partial y}\left[\left(\mu+\frac{\mu_{\mathrm{t}}}{\sigma_k}\right)\frac{\partial k}{\partial y}\right]+G_k+G_b-\rho\varepsilon \tag{16}$$

$$\frac{\partial(\rho u\varepsilon)}{\partial x}+\frac{\partial(\rho v\varepsilon)}{\partial y}=\frac{\partial}{\partial x}\left[\left(\mu+\frac{\mu_{\mathrm{t}}}{\sigma_\varepsilon}\right)\frac{\partial \varepsilon}{\partial x}\right]+\frac{\partial}{\partial y}\left[\left(\mu+\frac{\mu_{\mathrm{t}}}{\sigma_\varepsilon}\right)\frac{\partial \varepsilon}{\partial y}\right]+C_{1\varepsilon}\frac{\varepsilon}{k}(G_k+C_{3\varepsilon}G_b)-C_{2\varepsilon}\rho\frac{\varepsilon^2}{k} \tag{17}$$

where μ_{t} is the turbulent viscosity given by $\mu_{\mathrm{t}}=\rho C_\mu k^2/\varepsilon$, G_b is the buoyancy force given by $G_b=\beta g_i\frac{\mu_{\mathrm{t}}}{\sigma_{\mathrm{t}}}\frac{\partial T}{\partial x_i}$, and G_k is the rate of kinetic energy determined from

$$G_k=\mu_{\mathrm{t}}(\frac{\partial u_{\mathrm{i}}}{\partial x_{\mathrm{j}}}+\frac{\partial u_{\mathrm{j}}}{\partial x_{\mathrm{i}}})\frac{\partial u_{\mathrm{i}}}{\partial x_{\mathrm{j}}}-\frac{2}{3}\rho k\delta_{\mathrm{ij}}\frac{\partial u_{\mathrm{i}}}{\partial x_{\mathrm{j}}} \tag{18}$$

In addition, the values of constants are taken from Fluent theory guide as $C_{1\varepsilon}=1.44$, $C_{2\varepsilon}=1.92$, $C_{3\varepsilon}=1, C_{\mu}=0.09$, $\sigma_k=1.0$, and $\sigma_\varepsilon=1.3$ [28].

Eqs. (12)~(17) are solved via the CFD code Fluent [28]. The pressure-based coupled solver is employed to solve the conservation equations. The PRESTO method is employed for the

spatial discretization of pressure. In the vicinity of wall, the enhanced wall treatment is used to model the near-wall turbulence, and the first near-wall node is placed at the location of $y^+ \approx 1$. Computing convergence is achieved when the normalized residual for each equation is reduced to less than 10^{-4}.

3.2 Grid sensitivity analysis

In order to obtain the grid-independent results, an extensive testing is done to ensure that the obtained results are independent on the mesh density as well as the boundary size at cavity inlet and outlet.

A sample data from the grid sensitivity test is shown in Table 1. A total number of 8 grids are tested for the CFD analysis on the natural convection flow in a vertical cavity with its length (L) of 5 m and spacing (S) of 10 cm. 5 mesh sizes in the cavity are tested: 24×500, 24×1000, 34×1500, 45×1500 and 45×2000, and 3 boundary sizes at the cavity inlet and outlet are tested: W/S = 10, 20 and 40. The convective heat transfer in the cavity is evaluated using the CFD model described in Section 3.1. The temperatures of outdoor air, hot wall and cold wall are assumed to be 293 K (20°C), 323 K (50°C) and 313 K (40°C) respectively. The convective heat transfer coefficients in the cavity (h_o), at the hot wall (h_H) and cold wall (h_C) are evaluated by

$$h_o = \frac{q_{conv,h} + q_{conv,c}}{2(T_w - T_o)}, \qquad h_H = \frac{q_{conv,h}}{T_2 - T_o}, \qquad h_C = \frac{q_{conv,c}}{T_3 - T_o} \tag{19}$$

where $q_{conv,h}$ and $q_{conv,c}$ are the convective heat fluxes at the hot and cold walls respectively, in W/m^2.

Table 1 Sample data from the grid sensitivity analysis.

Grid No.	Total number of cells	Mesh size inside cavity	Inlet and outlet boundary size (W/S)	h_o	h_H	h_C

1	18944	24×500	10	3.86	4.09	3.53
2	32132	24×1000	10	3.84	4.06	3.51
3	43072	34×1000	10	3.79	3.99	3.49
4	77487	34×1500	10	3.78	3.98	3.47
5	103398	45×1500	10	3.77	3.97	3.48
6	144711	45×2000	10	3.77	3.97	3.47
7	107799	34×1500	20	3.79	3.97	3.49
8	193482	34×1500	40	3.77	3.97	3.47

The heat transfer coefficients h_o, h_H and h_C calculated by Eq. (19) are presented in Table 1. It is observed that the coefficients h_o, h_H and h_C gradually stabilize when the cavity mesh refines from 24×500 (Grid 1) to 45×2000 (Grid 6), and the coefficients vary within 0.02 when the inlet or outlet boundary size (W/S) increases from 10 (Grid 6) to 40 (Grid 8). The grid convergence index (GCI) of Grid 4 is evaluated using the Richardson extrapolation method [29]. The GCI of Grid 4 is found less than 0.5% for the three coefficients h_o, h_H and h_C, such that this grid is fine enough to perform CFD analysis.

3.3 Experimental validation of CFD model

After the grid sensitivity analysis, the CFD model is validated by the experiments carried out on the inclined and vertical cavities with natural ventilation flow.

3.3.1 Inclined cavity

In order to validate the CFD model, a laboratory experiment is carried out to study the airflow movement and convective heat transfer in the inclined roof. As shown in Fig. 4 (a), a roof apparatus is built up in laboratory. The ventilated roof cavity has a fixed length of 1.5 m and a width of 0.8 m. The cavity spacing (S) is adjusted by a scissor lift installed above the upper roof structure, as shown in Fig. 4 (b). The roof inclination (θ) is adjusted by the air cylinders

installed on both sides of the apparatus, as shown in Fig. 4 (c). The roof apparatus is placed in the laboratory with the constant temperature (T_i) of 297 K (24°C).

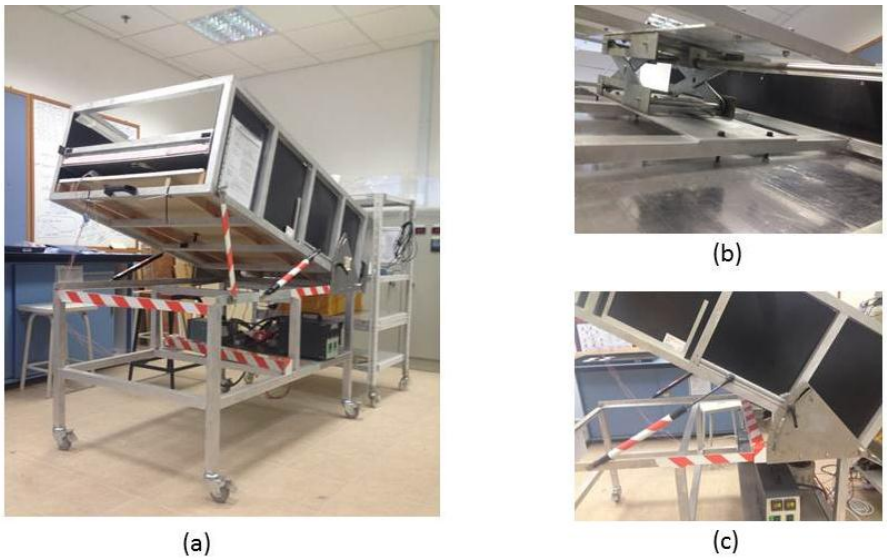

Fig. 4 (a) Experimental setup, (b) scissor lift and (c) air cylinder.

A schematic of the experimental setup and measurement is shown in Fig. 5. The upper roof structure consists of four layers from top to bottom, which are 1.5-cm thick gypsum board, 2.5-cm thick expanded polystyrene (EPS) foam, silicon rubber heater, and 0.3-cm thick aluminum plate respectively. The gypsum board presses the three underneath layers together to avoid the air leakage between layers. The silicon rubber heater provides electric heating power to the aluminum plate, and the heat loss from the upper side of heater is prevented by the EPS insulation foam. In addition, the silicon rubber heater consists of two heating sheets placed along the roof length direction. Each heating sheet is connected to a voltage controller so as to adjust the generated heat. The lower roof structure is formed by a 1.5-cm thick gypsum board with a thermal conductivity of 0.2 W/m K. The gypsum board has a comparable thermal resistance to a 15-cm thick reinforced concrete layer that is commonly used in Singapore residential roofs [30].

In the experiment, the temperature profiles of cavity upper and lower walls are measured by the resistance temperature detectors (RTDs) with the calibration errors within ±0.25°C. The

RTDs are placed along the roof length at 15 cm intervals. The air temperatures in the cavity are measured by the J-type thermocouples with calibration errors less than ±0.5°C in the temperature range of 15-65°C. Air velocities at cavity inlet and outlet are measured by the air velocity transducers (TSI model 8455) with an accuracy of ±2%. The heat flux emitted from the upper cavity wall is measured by the heat flux sensor (Hukseflux HFP01) with an accuracy of ±3%. All the measured data is collected by a personal computer installed with the data acquisition system.

Four experimental runs are performed to study the thermal performance of roof cavities at different cavity spacings ($S = 0.06$ m and 0.09 m) and inclinations ($\theta = 30°$ and 45°). Each run lasts for at least 8 hours, and the measured results are considered meaningful after the steady state of the roofing system is obtained. It typically takes 4-5 hours to reach the steady state, which is determined by checking whether all the cavity surface temperatures vary less than 0.5°C within half an hour. After the steady state is reached, the time-averaged roof surface temperatures are obtained over a 1.5-hour period with the data collected every 1 minute. The time-averaged air temperature and velocity in the cavity are obtained over a 20-minute period with the data collected every 1 second.

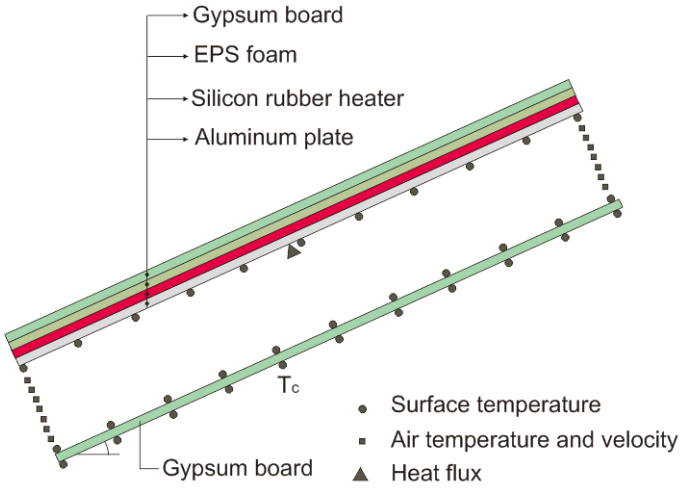

Fig. 5 Schematic of experimental roof and measurement.

The CFD model described in Section 3 is employed to simulate the airflow movement and temperature in the naturally ventilated cavity. The time-averaged temperature profiles of the cavity walls are used as model input. Comparisons are made between the simulated and measured results for the normalized air velocity V/V_{ave} and temperature $(T-T_o)/(T_2-T_o)$ at the cavity outlet for the four case studies: (a) $\theta = 30°$, $S = 6\,\text{cm}$; (b) $\theta = 30°$, $S = 9\,\text{cm}$; (c) $\theta = 45°$, $S = 6\,\text{cm}$; and (d) $\theta = 45°$, $S = 9\,\text{cm}$, as shown in Fig. 6 (a)-(d).

It is observed from Fig. 6 that the CFD model slightly over-predicts the air velocity near the cold wall and under-predicts the air temperature near the hot wall. One of the main reasons might be that the $k-\varepsilon$ turbulence model in Fluent does not take into account the effect of wall roughness and assumes both walls to be smooth. This leads to an over-predation in the induced airflow rate, especially at the cold wall side where the temperature difference between cavity wall and air is small and the buoyancy force is weak. Furthermore, the accelerated airflow rate impedes the growth of thermal boundary layers at both cavity walls, and leads to a weaker convective heat transfer in the cavity. In addition, the effects of wall roughness become less prominent in cavities with wider spacings, and thus better agreements are obtained in the cavities with the spacing of 9 cm than those of 6 cm.

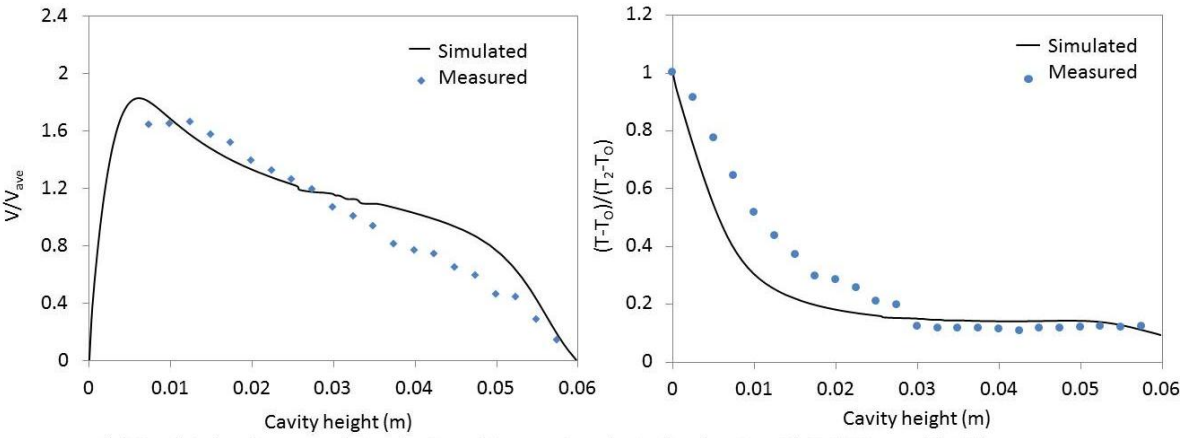

(a) Simulated and measured air velocity and temperature for inclined cavity with S=0.06 m and θ=30°

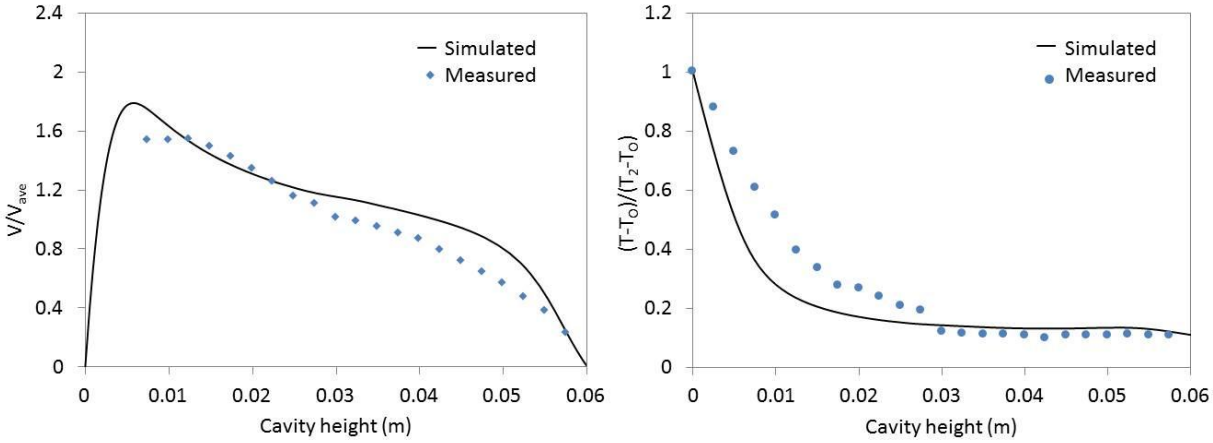

(b) Simulated and measured air velocity and temperature for inclined cavity with S=0.06 m and θ=45°

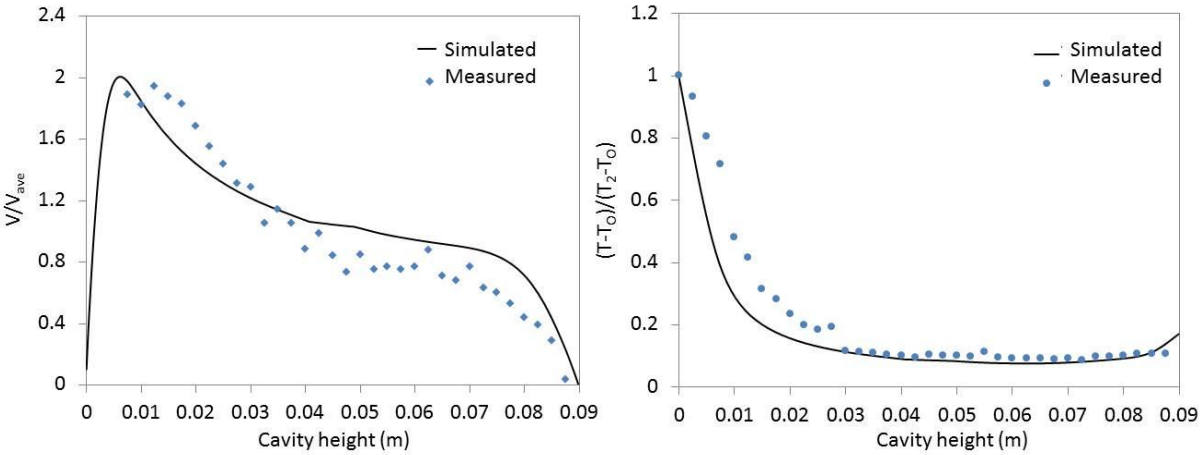

(c) Simulated and measured air velocity and temperature for inclined cavity with S=0.09 m and θ=30°

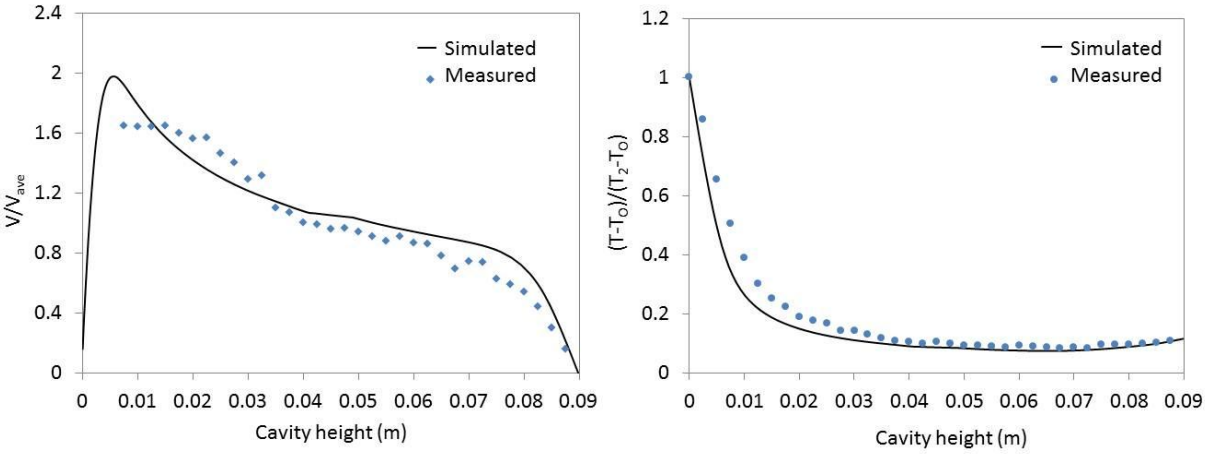

(d) Simulated and measured air velocity and temperature for inclined cavity with S=0.09 m and θ=45°

Fig. 6 Comparisons between simulated and measured air velocity and temperature in inclined cavity.

3.3.2 Vertical cavity

The experimental data obtained by Miyamoto et al. [31] in a vertical cavity is also used for the model validation. The 5-m long vertical cavity is composed of a heated plate and an adiabatic

plate, and the spacing between the two vertical plates is 5 cm. As shown in Fig. 7 (a)-(c), comparisons are made between the measured and simulated results for the normalized air velocity V/V_{ave} and temperature $(T-T_o)/(T_2-T_o)$ at three sections from the cavity inlet: $y/L=$ 0.773, 0.531 and 0.164. It is revealed that more satisfactory agreements between the measured and simulated results are obtained in the vertical cavity, compared to those obtained in the inclined cavity. It might be explained that the vertical cavity with a longer length of 5 m is more capable of controlling the heat transfer in the cavity and making it less disturbed by the indoor activities during the measurement, compared to the 1.5-m long inclined cavity.

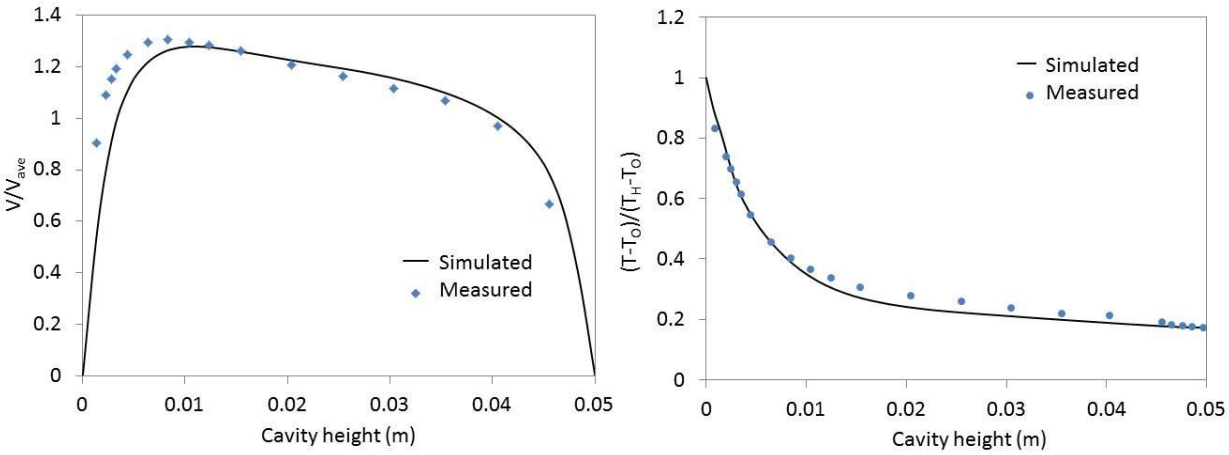

(a) Simulated and measured air velocity and temperature at the section y/L=0.773

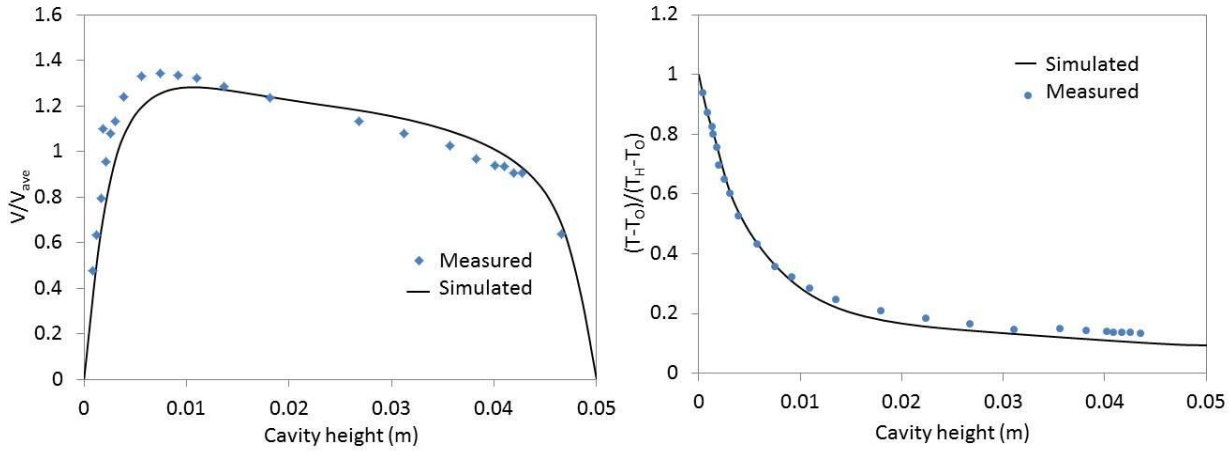

(b) Simulated and measured air velocity and temperature at the section y/L=0.531

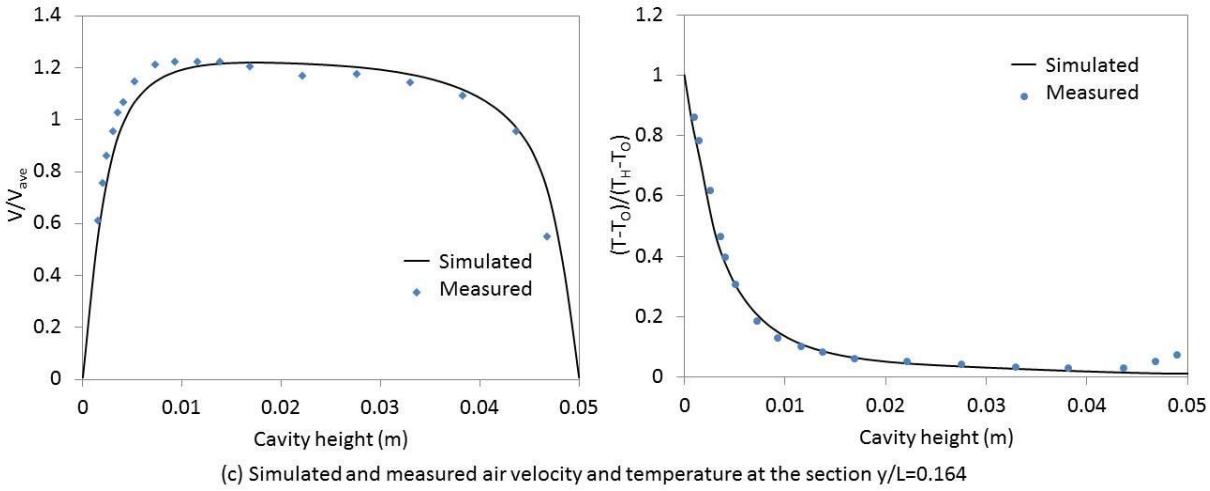

(c) Simulated and measured air velocity and temperature at the section y/L=0.164

Fig. 7 Comparisons between simulated and measured air velocity and temperature in vertical cavity.

3.4 Proposal of correlations

After validation, extensive studies are performed to evaluate the convective heat transfer in the naturally ventilated cavities using CFD analysis. The analyzed roofs have a fixed length of $L = 5\,\mathrm{m}$, different inclinations of θ = 15°, 30°, 45°, 60°, 75° and 90°, and different cavity spacings of S = 0.08 m, 0.1 m, 0.15 m and 0.2 m. Five sets of cavity wall temperatures are considered for the upper and lower cavity surfaces, and they are (a) T_2 = 313 K (40°C), T_3 = 303 K (30°C); (b) T_2 = 323 K (50°C), T_3 = 313 K (40°C); (c) T_2 = 333 K (60°C), T_3 = 323 K (50°C); (d) T_2 = 318 K (45°C), T_3 = 313 K (40°C); and (e) T_2 = 328 K (55°C), T_3 = 313 K (40°C). The free-stream air temperature T_0 remains at 293 K (20°C).

The overall heat transfer coefficients h_0 are predicted using Eq. (19) for the cavities under five sets of wall temperatures, as shown in Fig. 8 (a)-(e). It is revealed that the coefficient h_0 gradually increases with the larger inclination angle (θ) in all the cases. This is explained by the fact that when the cavity is inclined, a component of buoyancy force exists in the direction perpendicular to cavity surfaces as $\rho g \Delta V \cos\theta$, where ρ is the air density and ΔV is the volume of air displaced. This buoyancy component induces an outward flow away from the

heated cavity surfaces and impedes the growth of thermal boundary layer, thus the convective heat transfer in the cavity is weakened [13]. The effect of cavity spacing S on the coefficient h_o is more complex. From Fig. 8 (a)-(e), it is observed that the coefficient h_o slightly increases when the spacing S changes from 0.05 m to 0.08 m, but it gradually decreases when the spacing S changes from 0.08 m to 0.20 m. A similar trend is observed by other authors from their experimental measurements [3, 32] or CFD modeling analysis [13, 33] as well. It is explained that the convective heat transfer generally increases with the larger airflow rate in the cavity. When the spacing S is very small, the drag force due to friction becomes relative large, and thus impedes the airflow movement and convective heat transfer. However, when the spacing S is too wide, the temperature gradient in the heated air becomes too small to yield enough buoyancy force, and thus the rates of induced airflow and convective heat transfer are reduced. Therefore, an optimal cavity spacing of 0.08 m exists for the studied cavity, under which the convective heat transfer is the largest.

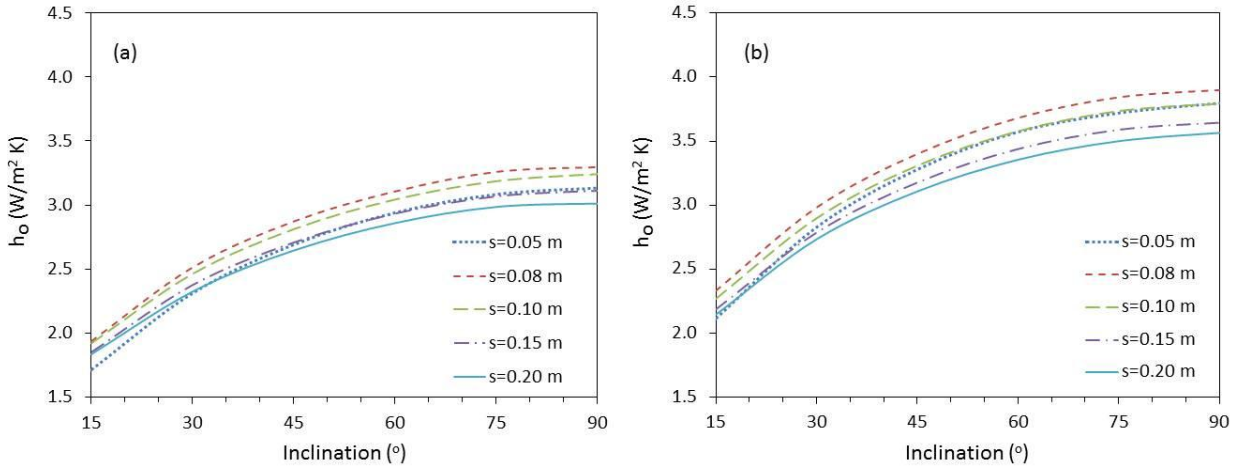

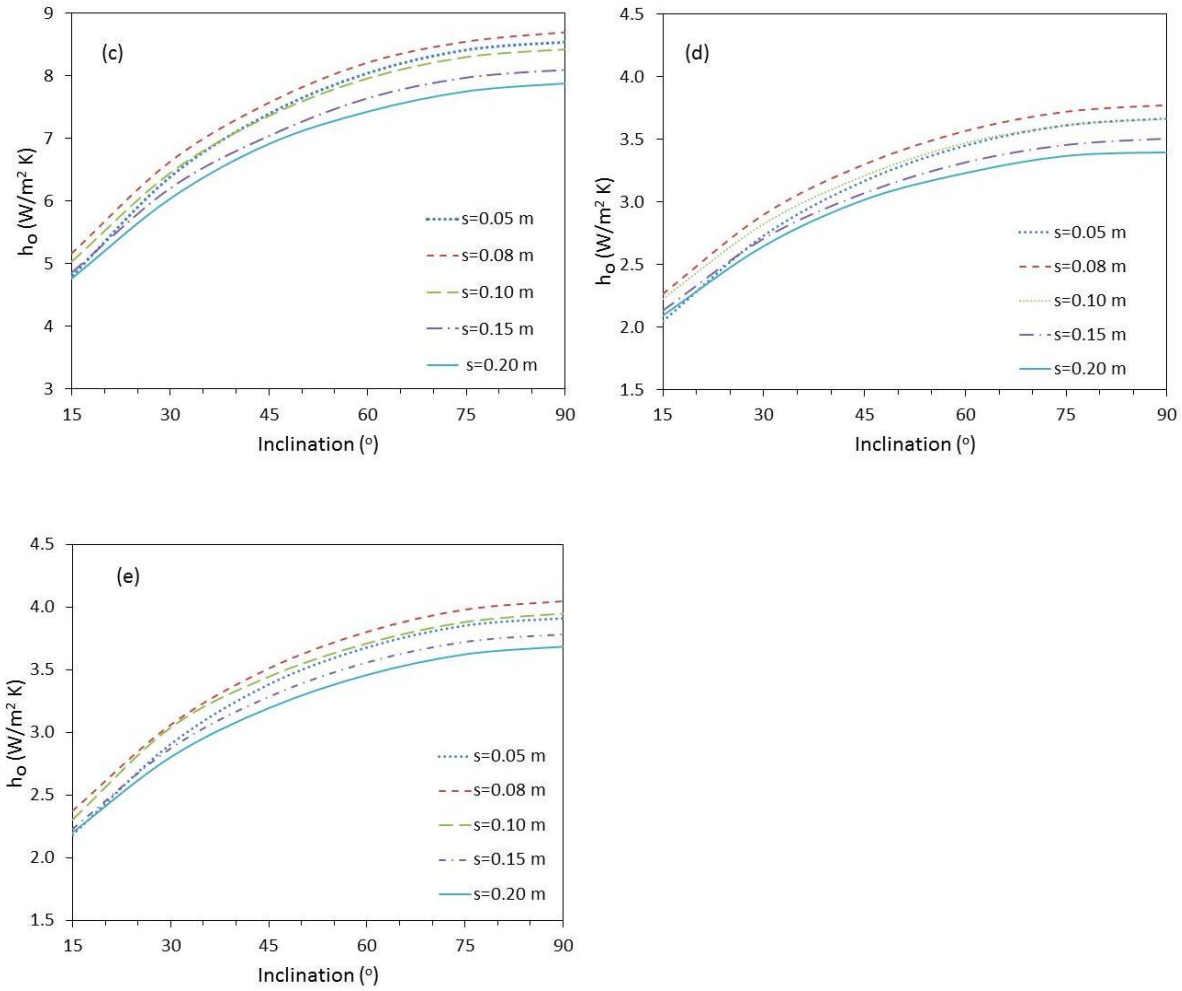

Fig. 8 Overall heat transfer coefficient h_0 in the cavity under five different wall temperatures (a) T_2 = 313 K, T_3 = 303 K; (b) T_2 = 323 K, T_3 = 313 K; (c) T_2 = 333 K, T_3 = 323 K; (d) T_2 = 318 K, T_3 = 313 K; and (e) T_2 = 328 K, T_3 = 313 K.

Based on simulation results, the Nusselt numbers (Nu_{H} and Nu_{C}) and Rayleigh numbers (Ra_{H} and Ra_{C}) at the upper and lower cavity walls are calculated using the following formulas.

$$Nu_{\mathrm{H}} = \frac{q_{\mathrm{conv,h}} S}{\lambda (T_2 - T_{\mathrm{o}})}, \qquad Nu_{\mathrm{C}} = \frac{q_{\mathrm{conv,c}} S}{\lambda (T_3 - T_{\mathrm{o}})} \tag{20}$$

$$Ra_{\mathrm{H}} = \frac{g\beta (T_2 - T_{\mathrm{o}}) S^3}{\nu \alpha}, \qquad Ra_{\mathrm{C}} = \frac{g\beta (T_3 - T_{\mathrm{o}}) S^3}{\nu \alpha} \tag{21}$$

where λ is the thermal conductivity of air in W/m K, and α is thermal diffusivity of air in m^2/K. Using the regression analysis in Matlab [34], the Nusselt number at the hot wall (Nu_H) is correlated to the modified Rayleigh number ($Ra_H \sin\theta$) and aspect ratio (S/L) with the average relative standard derivation (RSD) of 2% as

$$Nu_H = 0.0105 (Ra_H \sin\theta)^{0.41} (S/L)^{-0.29} \tag{22}$$

A similar correlation is obtained for the Nusselt number at the cold cavity wall Nu_C with the average RSD of 2% in the form

$$Nu_C = 0.0704 (Ra_C \sin\theta)^{0.35} (S/L)^{-0.04} \tag{23}$$

Therefore, the convective resistances at the upper and lower cavity walls become

$$r_H = (T_2 - T_o)/q_H = S/Nu_H\lambda = S/[0.0105\,\lambda\,(Ra_H \sin\theta)^{0.41}(S/L)^{-0.29}] \tag{24}$$

$$r_C = (T_3 - T_o)/q_C = S/Nu_C\lambda = S/[0.0704\,\lambda (Ra_C \sin\theta)^{0.35}(S/L)^{-0.04}] \tag{25}$$

The proposed correlations are valid for the natural convective flow with the overall Rayleigh number in the range $10^4 < Ra_o < 10^7$, where $Ra_o = g\beta(T_w - T_o)S^3/\nu\alpha$.

4. Analysis of computational accuracy

In this section, the computational accuracy of the developed model is analyzed. The model developed in Section 2 is implemented in Matlab [34] to estimate the transferred heat flux q_i, and the correlations proposed in Section 3 are employed to estimate the convective thermal resistances r_H and r_C.

The transferred heat flux q_i is evaluated by the developed model and a full CFD model. The full CFD model considers all the convective, radiative and conductive heat transfers as the

developed model. The input weather data for two models are the same, including the hourly solar irradiance (E), outdoor temperature (T_o) and indoor temperature (T_i). The solar irradiance (E) and temperature (T_o) shown in Fig. 9 are obtained from the field measurement on a sunny day in Singapore [30], and the indoor temperature (T_i) remains at 298 K (25°C). The studied roof has a length (L) of 5 m, inclination (θ) of 30° and cavity spacing (S) of 10 cm, according to the geometry of common ventilated roofs suggested in previous studies [5, 8, 9, 35]. The thermal properties of the studied roof are shown in Table 2. The solar reflectance and infrared emittance of the studied roof are assumed to be 0.8 and 0.9 respectively for the common non-reflective building materials. The thermal resistances of roof slabs and air films are taken from the building thermal code [22] and field experiment [30].

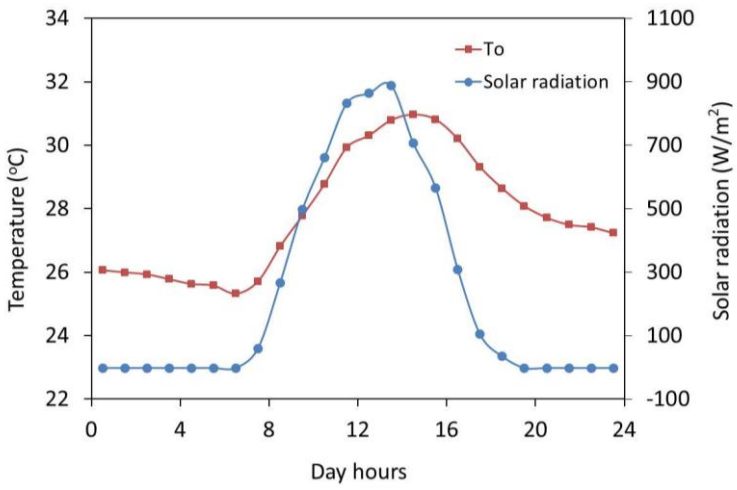

Fig. 9 Hourly outdoor air temperature and solar irradiance on a sunny day in Singapore.

Table 2 Thermal properties of the ventilated roof.

Solar absorptance of exterior roof surface	$\alpha = 0.8$
Infrared emittance of upper and lower cavity surfaces	$e_H = 0.9$, $e_C = 0.9$
Thermal resistances of exterior and interior air films	$r_e = 0.04\,\mathrm{m^2\,K/W}$, $r_i = 0.17\,\mathrm{m^2\,K/W}$
Thermal resistances of upper and lower roof slabs	$r_a = 0.036\mathrm{m^2\,K/W}$, $r_b = 0.104\,\mathrm{m^2\,K/W}$

The transferred heat fluxes q_i predicted by the developed and full CFD models are compared. As shown in Fig. 10, a very close agreement is obtained between the predictions of two models. It is thus concluded that the developed model with proposed correlations can provide an accurate prediction, and it requires much less computational effort than the full CFD model.

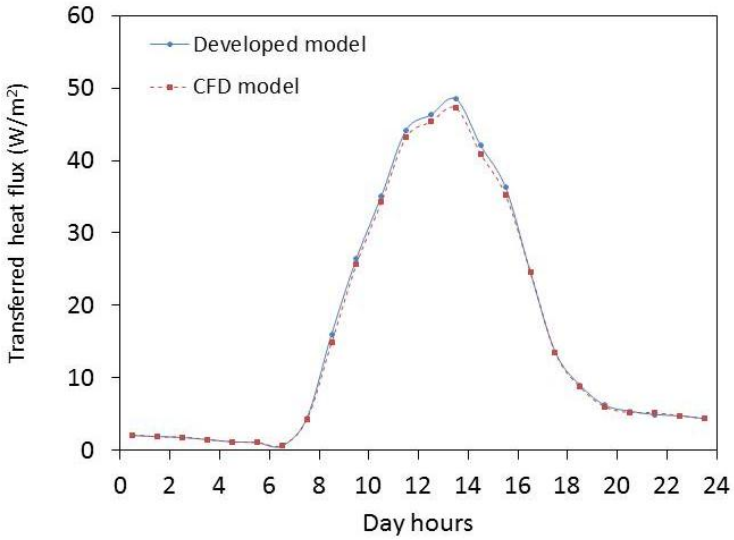

Fig. 10 Comparison between the developed and CFD models for the transferred heat flux.

5. Parametric studies

The developed model with the proposed correlations is used to study the impacts of key parameters on the transferred heat flux q_i. The investigated roof parameters include the solar absorptance of exterior surface (α), infrared emittance of cavity surface (e_H), thermal resistances of upper and lower roof slabs (r_a and r_b), cavity spacing (S) and roof inclination (θ). The roof has the same geometry and thermal properties as the one studied in Section 4, and it is exposed to solar irradiance (E) of 800 $\mathrm{W/m^2}$, outdoor temperature (T_o) of 303 K (30°C) and indoor temperature (T_i) of 298 K (25°C).

5.1 Impacts of solar absorptance and infrared emittance

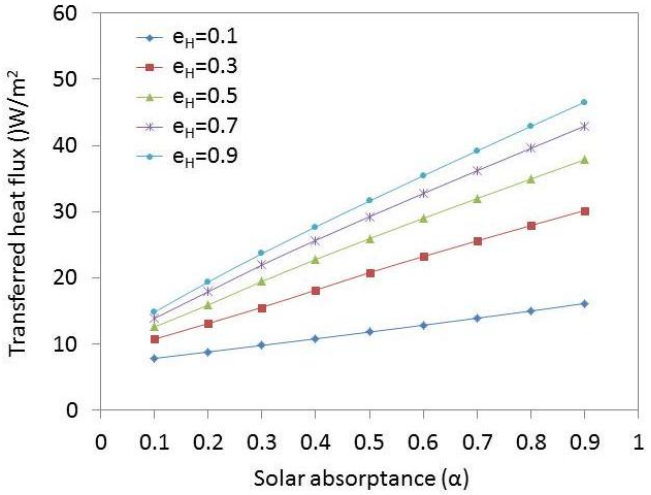

Fig. 11 Heat flux through the ventilated roof with varying solar reflectance and infrared emittance.

The transferred heat flux q_{i} is predicted for the ventilated roof with the solar absorptance of exterior surface (α) and infrared emittance of the upper cavity wall (e_{H}) varying from 0.1 to 0.9. As shown in Fig. 11, the transferred heat flux q_{i} increases significantly with the increase in the solar absorptance α. Every 0.1 increment in the solar absorptance α increases the transferred heat flux q_{i} by 0.9 and 4.5 $\mathrm{W/m^2}$ in the roofs with e_{H} of 0.1 and 0.9 respectively. Moreover, the transferred heat flux q_{i} reduces noticeably with the decrease in the thermal emittance e_{H}. When the thermal emittance e_{H} decreases from 0.9 to 0.1, the transferred heat flux q_{i} reduces by 8.3 and 31.7 $\mathrm{W/m^2}$ in the most reflective ($\alpha = 0.1$) and least reflective ($\alpha = 0.9$) roofs respectively. It is found that both the solar absorptance α and thermal emittance e_{H} have significant impacts on the transferred heat flux q_{i}.

5.2 Impacts of roof inclination and cavity aspect ratio

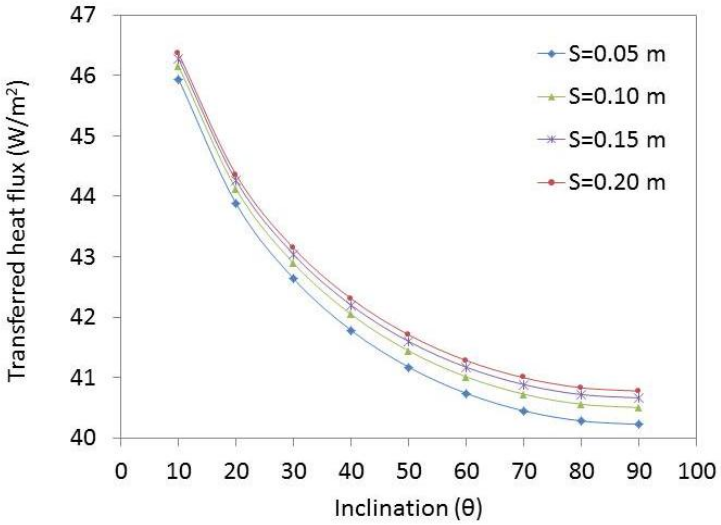

Fig. 12 Heat flux through the ventilated roof with different inclinations and cavity spacings.

The impacts of roof inclination and cavity spacing on the transferred heat flux are studied. As shown in Fig. 12, the transferred heat flux q_{i} decreases by approximately 6 $\mathrm{W/m^2}$ in all the roofs when the roof inclination (θ) increases from 10° to 90°. In addition, the impact of cavity spacing on the heat flux q_{i} is found very minimal. When the cavity spacing (S) increases from 0.05 to 0.2 m, the transferred heat flux q_{i} reduces slightly by less than 1 $\mathrm{W/m^2}$ in all the roofs. It is found that the impacts of roof inclination and cavity spacing on transferred heat flux are insignificant.

5.3 Impacts of thermal resistances of upper and lower roof slabs

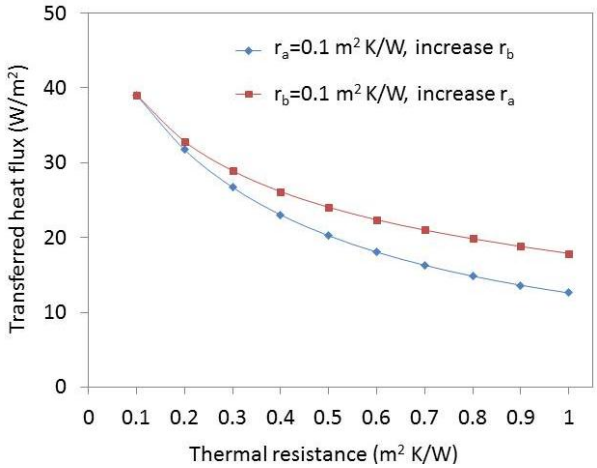

Fig. 13 Heat flux through ventilated roofs with varying thermal resistances of roof slabs.

The impacts of the thermal resistances of upper slab (r_a) and lower slab (r_b) are studied, by increasing the thermal resistance of one slab from 0.1 to 1 $\mathrm{m^2/K\,W}$ while keeping that of the other constant at 0.1 $\mathrm{m^2/K\,W}$. As shown in Fig. 13, increasing the thermal resistance of either roof slab can reduce the transferred heat flux q_i effectively. If r_a is kept at 1 $\mathrm{m^2/K\,W}$ and r_b increases from 0.1 to 1 $\mathrm{m^2/K\,W}$, the transferred heat flux q_i reduces from to 39 to 13 $\mathrm{W/m^2}$. In the reversed situation, the transferred heat flux q_i reduces less significantly from 39 to 18 $\mathrm{W/m^2}$ when r_a increases from 0.1 to 1 $\mathrm{m^2/K\,W}$. Therefore, it is more energy-efficient to place the thermal insulation layer adjacent to the lower roof slab than to the upper one.

Based on the parametric studies, it is found that the most influential parameters to the transferred heat flux q_i are the solar reflectance of roof (α) and infrared emittance of cavity surface (e_H), followed by the thermal resistance of lower slab (r_b), thermal resistance of upper slab (r_a), roof inclination (θ), and the cavity spacing (S).

6. Conclusion

In the present work, an efficient model is developed to predict the heat flux transferred through the naturally ventilated inclined roofs. Using the circuit transform theory, the thermal resistances due to the radiative and convective heat transfers in ventilated cavity are modeled, and a weighted average of the temperatures of sol-air, outdoor air and indoor air is introduced. Moreover, a CFD model is built up to simulate the turbulent natural convective heat transfer in the inclined cavity, and the CFD model is validated through experiments in inclined and vertical cavities with asymmetric heating. Based on the simulation results, correlations are proposed for the convective thermal resistances between air and the cavity walls. The proposed correlations are implemented in the developed model to predict the transferred heat flux q_i, and very close agreement is found between the predictions of the developed model and a full-CFD model.

Parametric studies are further carried out to evaluate the influences of key roof parameters on the heat flux transferred through the ventilated roofs. The most influential roof parameters are the solar reflectance of exterior surface (α) and the infrared emittance of cavity surface (e_{H}), followed by the thermal resistance of lower slab (r_{b}), thermal resistance of upper slab (r_{a}), roof inclination (θ) and cavity spacing (S).

The developed model and proposed correlations are applicable to the design of and energy analysis other open-ended cavities in the buildings as well, such as the ventilated façades, solar chimneys, and building-integrated photovoltaics.

Acknowledgement

The authors highly appreciate the scholarship provided by the Energy Research Institute @ NTU.

Nomenclature

$C_{1\varepsilon}, C_{2\varepsilon}, C_{3\varepsilon}, C_{\mu}$	empirical constants in the $k-\varepsilon$ turbulence model
E	solar irradiance ($\mathrm{W/m^2}$)
e_{H} , e_{C}	infrared emittance of upper and lower cavity surfaces
Gr_L	Grashof number based on cavity length
g	acceleration of gravity ($\mathrm{m/s^2}$)
h_{o} , h_{H} , h_{C}	convective heat transfer coefficients between air and the overall cavity, hot and cold walls ($\mathrm{W/m^2\,K}$), Eq. (19)
k	turbulent kinetic energy ($\mathrm{m/s^2}$)
L	length of roof or cavity (m)
Nu_{o} , Nu_{H} , Nu_{C}	Nusselt numbers in the cavity, at the hot and cold walls

p	air pressure (Pa)
Pr	Prandtl number
$q_{\text{cond,u}}$, $q_{\text{cond,l}}$	conductive heat fluxes within the upper and lower roof slabs (W/m^2)
$q_{\text{conv,h}}$, $q_{\text{conv,c}}$	convective heat fluxes at the upper and lower surfaces of ventilated cavity (W/m^2)
q_{o} , q_{i}	coupled convective and radiative heat fluxes at the exterior and interior surfaces of roof (W/m^2)
q_{rad}	radiative heat transfer between the upper and lower surface of cavity (W/m^2)
r_1, r_2, r_3	transformed thermal resistances in ventilated cavity ($\text{m}^2 \cdot \text{K/W}$)
r_{rad}	thermal resistance due to radiation between upper and lower cavity walls (m^2 K/W)
$r_{\text{a}}, r_{\text{b}}$	thermal resistances of upper and lower cavity slabs ($\text{m}^2 \cdot \text{K/W}$)
$r_{\text{e}}, r_{\text{i}}$	thermal resistances of exterior and interior air films ($\text{m}^2 \cdot \text{K/W}$)
$r_{\text{H}}, r_{\text{C}}$	thermal resistances due to convection between air and the upper and lower cavity surfaces ($\text{m}^2 \cdot \text{K/W}$)
Ra_{o} , Ra_{H} , Ra_{C}	Rayleigh numbers in the cavity, at the hot and cold walls
S	cavity spacing (m)
T_1, T_2, T_3, T_4	surface temperatures of ventilated roof slabs (K or °C)
T_{a}	sol-air temperature (K), Eq. (1)
T_{m}	introduced node temperature in the Y-mesh thermal circuit (K)
T_{m}	introduced node temperature in the Y-mesh thermal circuit (K)
$T_{\text{o}}, T_{\text{i}}$	outdoor and indoor air temperatures (K or °C)
u, v	air flow velocity in x and y direction (m/s)
W	domain size at the cavity inlet and outlet (m)
Greek letters	

α	solar absorptance of ventilated roof, or thermal diffusivity ($\lambda / \rho C_p$)
ε	dissipation rate of turbulent kinetic energy (m^2/s^3)
σ	Stefan-Boltzmann constant, 5.67×10^{-8} (W/m^2K^4)
σ_k, σ_ε	empirical constants in $k-\varepsilon$ turbulence model
λ	thermal conductivity of air (W/m K)
ν	kinematic viscosity of air (m^2/s)
μ	dynamic viscosity of air (kg/m s)
ρ	density of air (kg/m^3)
θ	cavity inclination from the horizontal plane (°)

Appendix A. Derivation of the Δ-Y circuit transform

The Δ-Y transform was developed by Kennelly [20] in 1899 to simplify the analysis of electrical circuits. In this study, the Δ-Y transform is employed to convert the triangular circuit among temperature nodes into an equivalent Y-circuit.

As shown in Fig. 2, the resistances r_H, r_C and r_{rad} connecting the temperature nodes T_2, T_3 and T_o in the triangular circuit can be transferred to the resistances r_1 , r_2 and r_3 in the Y-circuit. In order to relate r_1 , r_2 and r_3 to r_H, r_C and r_{rad}, the corresponding impedances between temperature nodes in the two circuits are compared. The impedance between two temperature nodes is calculated by assuming the third node is disconnected. For example, the impedance between T_2 and T_3 with T_o disconnected in the triangular circuit is

$$r_\Delta(T_2,T_3) = r_{rad} \parallel (r_H + r_C) = 1/[1/r_{rad} + 1/(r_H + r_C)] = r_{rad}(r_H + r_C)/(r_{rad} + r_H + r_C) \qquad (A.1)$$

The corresponding impedance between T_2 and T_3 with T_o disconnected in the Y-circuit is

$$r_{\mathrm{Y}}(T_2, T_3) = r_1 + r_2 \tag{A.2}$$

Let $r_{\Delta}(T_2, T_3) = r_{\mathrm{Y}}(T_2, T_3)$, the relationship between r_1, r_2 and r_{H}, r_{C}, r_{rad} is obtained as

$$r_1 + r_2 = r_{\mathrm{rad}}(r_{\mathrm{H}} + r_{\mathrm{C}})/(r_{\mathrm{rad}} + r_{\mathrm{H}} + r_{\mathrm{C}}) \tag{A.3}$$

Similarly, we obtain the following relationships from the impedances between T_2 and T_{o}, T_{o} and T_3 as

$$r_1 + r_3 = r_{\mathrm{H}}(r_{\mathrm{rad}} + r_{\mathrm{C}})/(r_{\mathrm{rad}} + r_{\mathrm{H}} + r_{\mathrm{C}}) \tag{A.4}$$

$$r_2 + r_3 = r_{\mathrm{C}}(r_{\mathrm{rad}} + r_{\mathrm{H}})/(r_{\mathrm{rad}} + r_{\mathrm{H}} + r_{\mathrm{C}}) \tag{A.5}$$

Thereby, solving Eqs. (A.3)-(A.5) for the thermal resistances r_1, r_2 and r_3 yields that

$$r_1 = r_{\mathrm{H}} r_{\mathrm{rad}}/(r_{\mathrm{H}} + r_{\mathrm{rad}} + r_{\mathrm{C}}), \quad r_2 = r_{\mathrm{C}} r_{\mathrm{rad}}/(r_{\mathrm{H}} + r_{\mathrm{rad}} + r_{\mathrm{C}}), \quad r_3 = r_{\mathrm{H}} r_{\mathrm{C}}/(r_{\mathrm{H}} + r_{\mathrm{rad}} + r_{\mathrm{C}}) \tag{A.6}$$

Reference

[1] A. Dimoudi, A. Androutsopoulos, S. Lykoudis, Summer performance of a ventilated roof component, Energy and Buildings, 2006;38: 610-617.

[2] W. Puangsombut, J. Hirunlabh, J. Khedari, B. Zeghmati, M. M. Win, Enhancement of natural ventilation rate and attic heat gain reduction of roof solar collector using radiant barrier, Building and Environment, 2007;42: 2218-2226.

[3] C.-m. Lai, J. Y. Huang, J. S. Chiou, Optimal spacing for double-skin roofs, Building and Environment, 2008;43: 1749–1754.

[4] P.-C. Chang, C.-M. Chiang, C.-M. Lai, Development and preliminary evaluation of double roof prototypes incorporating RBS (radiant barrier system), Energy and Buildings, 2008;40: 140-147.

[5] L. Susanti, H. Homma, H. Matsumoto, A naturally ventilated cavity roof as potential benefits for improving thermal environment and cooling load of a factory building, Energy and Buildings, 2011;43: 211-218.

[6] S. Roels, M. Deurinck, The effect of a reflective underlay on the global thermal behaviour of pitched roofs, Building and Environment, 2011;46: 134-143.

[7] P. H. Biwole, M. Woloszyn, C. Pompeo, Heat transfers in a double-skin roof ventilated by natural convection in summer time, Energy and Buildings, 2008;40:1487-1497.

[8] N. Chami, A. Zoughaib, Modeling natural convection in a pitched thermosyphon system in building roofs and experimental validation using particle image velocimetry, Energy and Buildings, 2010;42:1267-1274.

[9] A. Gagliano, F. Patania, F. Nocera, A. Ferlito, A. Galesi, Thermal performance of ventilated roofs

during summer period, Energy and Buildings, 2012;49:611-618.
[10] W. Miller, M. Keyhani, T. Stovall, A. Youngquist, Natural convection heat transfer in roofs with above-sheathing ventilation, Thermal Performance of the Exterior Envelopes of Buildings, 2007.
[11] L. F. A. Azevedo, E. M. Sparrow, Natural convection in open-ended inclined channels, Journal of Heat Transfer, 1985;107: 893-901.
[12] E. Sanvicente, S. Giroux-Julien, C. Ménézo, H. Bouia, Transitional natural convection flow and heat transfer in an open channel, International Journal of Thermal Sciences, 2013;63: 87-104.
[13] A. S. Alzwayi, M. C. Paul, Transition of free convection flow inside an inclined parallel walled channel: Effects of inclination angle and width of the channel, International Journal of Heat and Mass Transfer, 2014;68: 194-202.
[14] S. A. M. Said, M. A. Habib, H. M. Badr, S. Anwar, Turbulent natural convection between inclined isothermal plates, Computers & Fluids, 2005;34:1025-1039.
[15] G. E. Lau, E. Sanvicente, G. H. Yeoh, V. Timchenko, M. Fossa, C. Ménézo, S. Giroux-Julien, Modelling of natural convection in vertical and tilted photovoltaic applications, Energy and Buildings, 2012;55: 810-822.
[16] M. Ciampi, F. Leccese, G. Tuoni, Energy analysis of ventilated and microventilated roofs, Solar Energy, 2005;79:183-192.
[17] W. M. Rohsenow, J. P. Hartnett, E. N. Ganić, Handbook of heat transfer fundamentals, 2nd ed, McGraw-Hill Inc.; 1985.
[18] M. Ciampi, F. Leccese, G. Tuoni, Ventilated facades energy performance in summer cooling of buildings, Solar Energy, 2003;75:491-502.
[19] F. P. Incropera, D. P. DeWitt, Fundamentals of heat and mass transfer. New York: Wiley, 5th ed., 2002.
[20] A. E. Kennelly, Equivalence of triangles and stars in conducting networks, Electrical World and Engineer, Electrical World and Engineer, 1989;34:413–414.
[21] Chapter 25, ASHRAE, Heat, Air, and Moisture Control in Building Assemblies-Fundamentals, American Society of Heating, Refreigeration and Air-Conditioning Engineers, 2009.
[22] Code on Envelope Thermal Performance for Buildings, Building Construction Authority, Singapore, 2008.
[23] A. S. Alzwayi, M. C. Paul, Effect of width and temperature of a vertical parallel plate channel on the transition of the developing thermal boundary layer, International Journal of Heat and Mass Transfer, 2013;63:20-30.
[24] C. R. Maliska, F. Marcondes, Elliptic calculations of natural convection flows in arbitrary channels, in 8th Int. Conf. on Laminar and Turbulent Flow, Swansea, UK, 1993; 388-399.
[25] B. Morrone, A. Campo, O. Manca, Optimum plate separation in vertical parallelplate channels for natural convective flows: incorporation of large spaces at the channel extremes, International Journal of Heat and Mass Transfer, 1997;40: 993-1000.
[26] A. Campo, O. Manca, B. Morrone, Numerical analysis of partially heated vertical parallel plates in natural convective cooling, Numerical Heat Transfer, Part A, 1999;36: 129-151.
[27] B. B. E. Launder, D. D. B. Spalding, Lectures in Mathematical Models of Turbulence: Academic Press, 1972.
[28] Ansys Fluent Theory Guide 14.0, Fluent Inc.
[29] Procedure for estimation and reporting of uncertainty due to discretization in CFD Applications, Journal of Fluids Engineering, 2008;130: 078001-078001.
[30] S. Tong, H. Li, K. T. Zingre, M. P. Wan, V. W. C. Chang, S. K. Wong, W. B. T. Toh, I. Y. L. Lee, Thermal performance of concrete-based roofs in tropical climate, Energy and Buildings, 2014;76: 392-401.
[31] M. Miyamoto, Y. Katoh, J. Kurima, H. Sasaki, Turbulent free convection heat transfer from vertical parallel plates, In: Proceeding of the 8th international heat transfer conference, 1986;593–1598.
[32] N. Onur, M. Sivrioğlu, M. K. Aktaş, An experimental study on the natural convection heat transfer between inclined plates (Lower plate isothermally heated and the upper plate thermally insulated as well as unheated), Heat and Mass Transfer, 1997;32: 471-476.
[33] S. Baskaya, M. K. Aktas, N. Onur, Numerical simulation of the effects of plate separation and inclination on heat transfer in buoyancy driven open channels, Heat and Mass Transfer, 1999;35:

273-280.
[34] D. C. Hanselman, B. Littlefield, Mastering MATLAB 6: a comprehensive tutorial and reference, Prentice Hall, 2001.
[35] G. Villi, W. Pasut, M. Carli, CFD modelling and thermal performance analysis of a wooden ventilated roof structure, Building Simulation, 2009;2: 215-228.